Nonlinear Photocarrier Dynamics in Multilayer WSe_2 Induced By Intense Terahertz Pulses

VIELA GUAY,[1] NATHAN JOHNSON,[1], YUE ZHANG[2], AREND M. VAN DER ZANDE,[2,3] SPENCER G. THORP,[1] MATTHEW GRAHAM,[1] AND YUN-SHIK LEE,[1,*]

[1]*Department of Physics, Oregon State University, 103 SW Memorial Place, Corvallis, OR 97331, USA*
[2]*Mechanical Science and Engineering, University of Illinois at Urbana Champaign, 1201 W. University Avenue, Urbana, IL 61801, USA*
[3]*Materials Research Lab, University of Illinois at Urbana Champaign, 104 S Goodwin Ave, Urbana, IL 61801, USA*
[*]*leeys@oregonstate.edu*

Abstract: Non-equilibrium photocarriers in multilayer WSe_2 injected by femtosecond laser pulses exhibit extraordinary nonlinear dynamics in the presence of intense THz fields. The THz absorption in optically excited WSe_2 rises rapidly in the low THz field regime and gradually ramp up at high intensities. The strong THz pulses drive the photocarriers into sidebands of higher mobility and release trapped charge carriers, which consequently enhance the transient conductivity of WSe_2. The spectrally analyzed conductivity reveals distinctive features, indicating that the photocarriers undergo resonant interactions such as carrier-photon scattering.

1. Introduction

Transition metal dichalcogenides (TMDCs) are 2D semiconductors of unique electronic structure, possessing distinctive electronic and optical properties such as a direct bandgap [1, 2], strong spin-orbit coupling [3, 4], degenerate valleys at band edges [5–8], spin-dependent photocarrier dynamics [9], and exciton resonances [10–13]. The electronic structure of a TMDC changes with thickness [14], and in particular, the indirect bandgap in bulk MoS_2 and WSe_2 is widened with decreasing thickness, which leads to a transition to direct bandgap in a single layer [1, 2, 15]. A wide range of studies have demonstrated appealing properties of TMDCs for promising applications in nanoelectronics and optoelectronics [16].

TMDCs are attractive base materials for high-speed and high-frequency photonic devices [17, 18]. Time-resolved spectroscopy with electromagnetic waves has provided crucial insight into the ultrafast carrier dynamics in TMDCs. The experimental results show that the microscopic processes of the ultrafast carrier dynamics such as exciton formation and relaxation [19–21], resonant quantum transitions [22], and Auger scattering [23] take place on a sub-picosecond time scale. Time-resolved terahertz (THz) spectroscopy is a powerful tool to observe the temporal evolution of the carrier dynamics in TMDCs because of its high sensitivity to electrical conductivity changes [24, 25]. It is also capable of measuring the complex refractive index in a broad spectrum, providing comprehensive information about the electron configuration and many-body interactions in TMDCs [26–29]. The strong interaction of THz waves with photocarriers enables the development of new THz photonic devices for high-sensitivity THz modulation with optical control [30–32].

In this study, we investigate high-field photocarrier dynamics in large-grain multilayer WSe_2, employing time-resolved high-field THz spectroscopy. Control of the TMDC electronic structure via electric field can provide promising platforms not only for nanoelectronic and spintronic applications [33, 34], but also for exploring fundamental physical processes such as phase transitions and many-body interactions [33, 35, 36]. High-field THz spectroscopy is an effective tool for manipulating carrier dynamics in photoexcited materials [37, 38], yet only a handful of studies have exploited the method to control the optical and electronic properties

of TMDCs [34, 39]. We demonstrate that intense THz fields induce precipitous changes in photocarrier dynamics in WSe_2.

2. Experiments

We exfoliated the large area WSe_2 sample from bulk and transferred onto a sapphire substrate. Characterization of the sample substantiates its large grain size and high quantum yield of photoluminescence. The optical microscope image in Fig. 1a shows the monolayer and multilayer regions of the sample. A THz transmission image of the optically excited multilayer region of 25 layers is also shown.

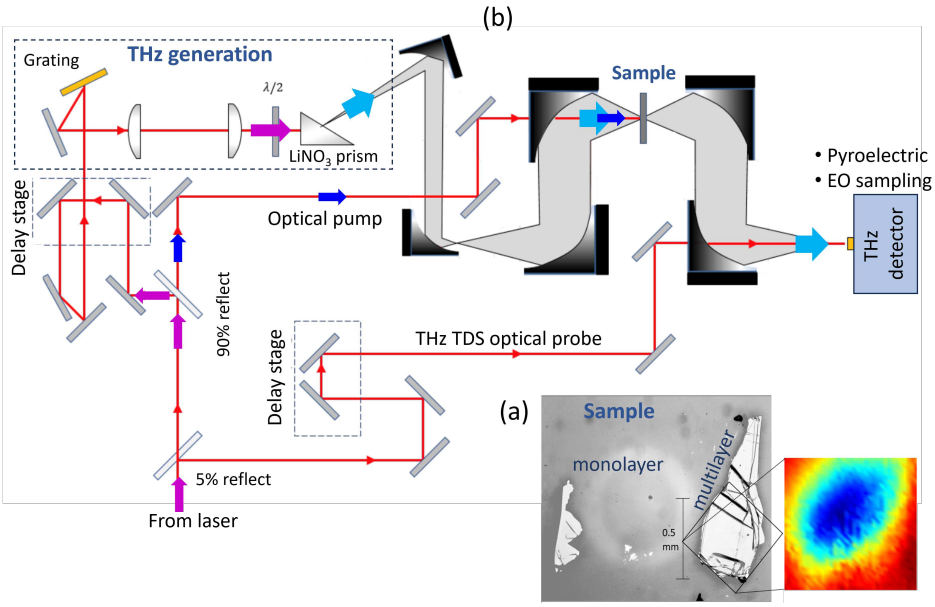

Fig. 1. (a) Optical microscopy image of the WSe_2 sample (left) and THz transmission scan highlighting the optically excited multilayer region (right) (b) Schematic of the experimental setup for time-resolved high-field THz spectroscopy of photocarriers. THz pulses are generated by optical rectification in a lithium niobate prism and measured by two detectors, pyroelectric detector for pulse energy measurements and electro-optic sampling for waveform measurements.

Figure 1b shows a schematic of the experimental setup for time-resolved THz spectroscopy of photocarriers in WSe_2. We generate intense single-cycle THz pulses by tilted-pulse-front optical rectification in a Mg:$LiNbO_3$ prism using a 1-kHz regenerative amplifier (wavelength, 800 nm; pulse energy, 1 mJ; pulse duration, 100 fs) [38, 40]. THz pulses are focused to near diffraction limit (beam waist, 0.4 mm) onto the sample by off-axis parabolic mirrors. The THz spectrum is centered at 0.7 THz and has a broadband of 0.7 THz FWHM bandwidth. The peak field of the THz pulses reaches 1.1 MV/cm at an optical pulse energy of 1 mJ. We measure THz pulse energy using a pyroelectric detector and obtain THz waveforms employing electro-optic (EO) sampling in a 1-mm ZnTe crystal. A small portion of the regenerative amplifier output and its second harmonic generation in a BBO crystal are used for optical excitation of the WSe_2 sample at 800 and 400 nm, respectively.

3. Photocarrier Relaxation In Intense THz Fields

THz photon energy being considerably smaller than the bandgap of WSe_2, THz absorption is negligible in the extremely thin dielectric medium. Optical excitations, however, make qualitative changes in the THz properties of WSe_2, where THz radiation strongly interacts with photocarriers. We observe the photocarrier relaxation in the WSe_2 sample which is optically excited by either 400-nm or 800-nm 100-fs optical pulses, using optical-pump/THz-probe spectroscopy. The photon energies are above and below the monolayer bandgap of ~1.7 eV, respectively, while both exceed the multilayer bandgap of ~1.4 eV. Figure 2 shows that an optical excitation instantly induces large THz absorption in WSe_2, and the photocarriers undergo slow relaxation in hundreds of picosecond time scale. The relaxation time is 395 ps at 400 nm, which is significantly longer than the relaxation time 263 ps at 800 nm. The hot-carrier relaxation may be prolonged by defect-mediated trapping and phonon bottlenecks [41, 42].

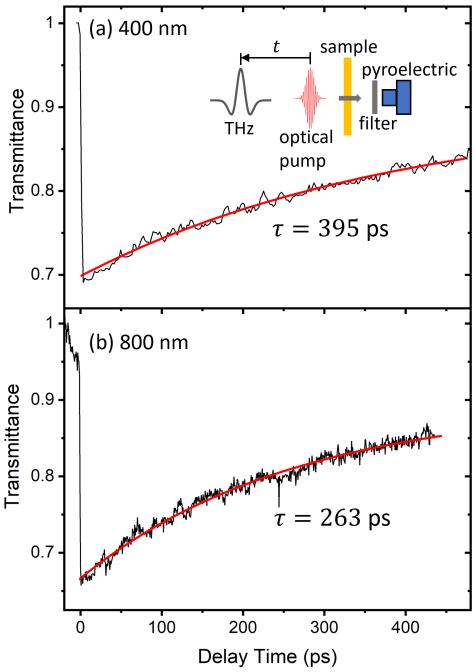

Fig. 2. Time-resolved THz transmittance of the multilayer WSe_2 sample excited by a 100-fs optical pump, with inset schematic of the optical-pump/THz-Probe experiment. The optical pump wavelength is either (a) 400 nm or (b) 800 nm, where the pump fluence is 710 μJ/cm^2 and 770 μJ/cm^2, respectively. The relaxation time is 395 ps at 400 nm and 263 ps at 800 nm.

In the presence of strong THz fields, photocarrier dynamics in WSe_2 exhibit distinctive nonlinear effects depending on the THz intensity. Figure 3 presents the time-resolved THz transmission through the sample at various peak-field amplitudes of the THz pulses ranging from 110 to 1100 kV/cm for (a) 400-nm and (b) 800-nm optical pumping for the first 10 picoseconds. The optical pump fluence is set to 730 μJ/cm^2 at 400 nm and 770 μJ/cm^2 at 800 nm. The optically induced THz absorption shows nonlinear responses at both optical pump wavelengths. The THz transmittance reduces from 57% at 110 kV/cm to 52% at 1100 kV/cm for the 400-nm pumping and from 63% to 58% for the 800-nm pumping.

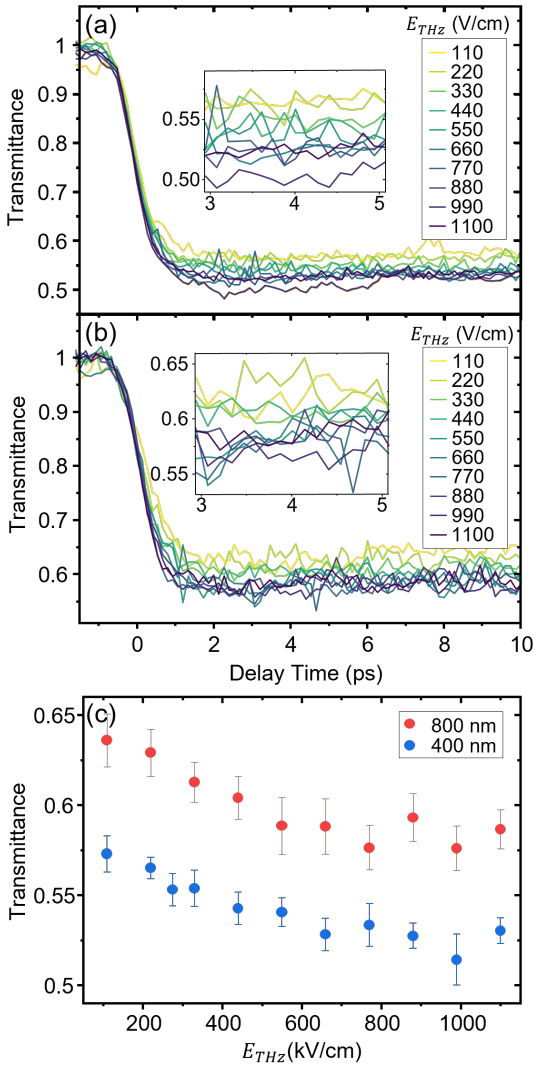

Fig. 3. Time-resolved THz transmittance of WSe_2 at the peak THz field amplitude of 110, 220, 330, 440, 550, 660, 770, 990 and 1100 kV/cm for (a) 400-nm and (b) 800-nm optical pumping. The optical pump fluence is 730 μJ/cm^2 at 400 nm and 770 μJ/cm^2 at 800 nm. (c) Averaged THz transmittance between 3 and 5 ps versus peak THz field amplitude for 400-nm and 800-nm optical pumping

The nonlinear THz transmission depending on the field amplitude is shown in Fig. 3c. The THz pulses produce similar nonlinear effects at both optical excitation wavelengths. The THz transmittance gradually decreases up to 600 kV/cm as the THz field strength increases, and the nonlinear response saturates at the higher fields for the both optical pump wavelengths. The nonlinear THz absorption is stronger for 400-nm pumping than for 800-nm pumping. We speculate that the hot carriers of high density injected by 400-nm pumping are more efficient for carrier multiplication than the relatively cold carriers of 800-nm pumping. [43] It is noteworthy that the field induced opacity in WSe_2 is extraordinary, considering that strong THz fields commonly induce transparency in conventional 3D semiconductors such as Si, Ge and GaAs [44–47].

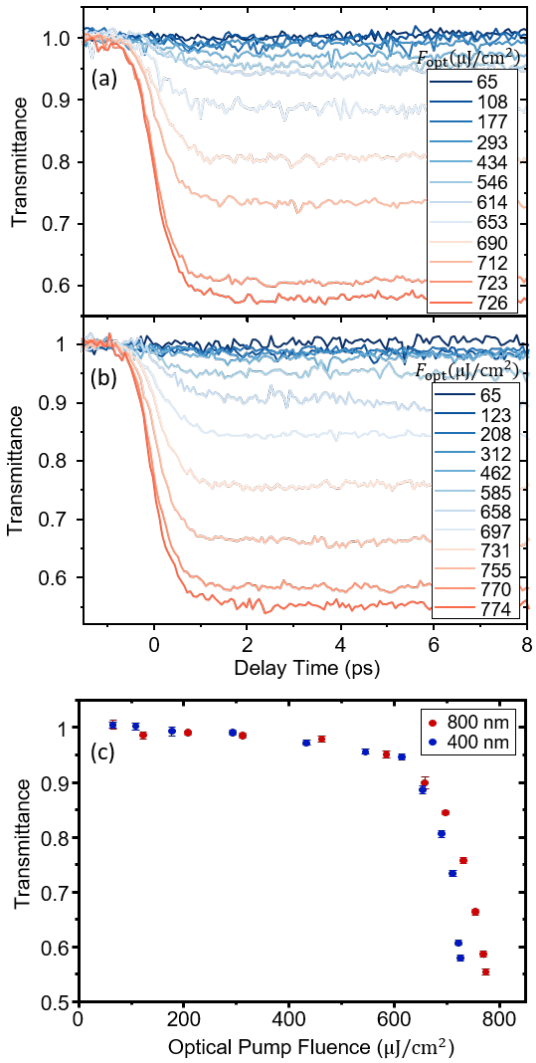

Fig. 4. Time-resolved THz transmittance of WSe_2 at various optical pump fluences for (a) 400-nm and (b) 800-nm pumping when the peak THz field amplitude is set to 1100 kV/cm. (c) Averaged THz transmittance between 3 and 5 ps versus optical pump fluence for 800-nm and 400-nm pumping

Figure 4 presents the time-resolved THz transmission through the sample at various optical pump fluences for (a) 400-nm and (b) 800-nm pumping, where the incident THz pulse is held at a fixed field strength of 1100 kV/cm. The THz absorption induced by optical pumping demonstrates strong nonlinear optical effects at both wavelengths. Figure 4c shows that the THz transmittance undergoes a gradual yet slight decline up to 600 μJ of the optical pump fluence, while plunging more than 40% above the threshold. The nonlinear behavior of the THz absorption and the stronger effect for 400-nm pumping indicates that the WSe_2 sample experiences carrier multiplication due to the high density of the hot carriers. [43]

4. High-Field THz Time Domain Spectroscopy

We performed high-field THz time-domain spectroscopy for an extensive investigation of the nonlinear THz responses in the WSe_2 sample. Figure 5a shows the waveforms transmitted through the sample excited by 400-nm pump pulses at the peak THz-field amplitude from 110 to 1100 kV/cm, and the corresponding transmittance spectra are shown in Fig 5b. The decrease in transmission as the THz-field strength increases is notable in Fig. 5b. The inset of Fig. 5b presents the spectrally integrated transmittance as a function of peak THz-field strength, showing that the transmission rapidly decreases in the low field regime, while gradually declining at higher THz field amplitudes. The results are consistent with the time-resolved measurements shown in Fig 3c.

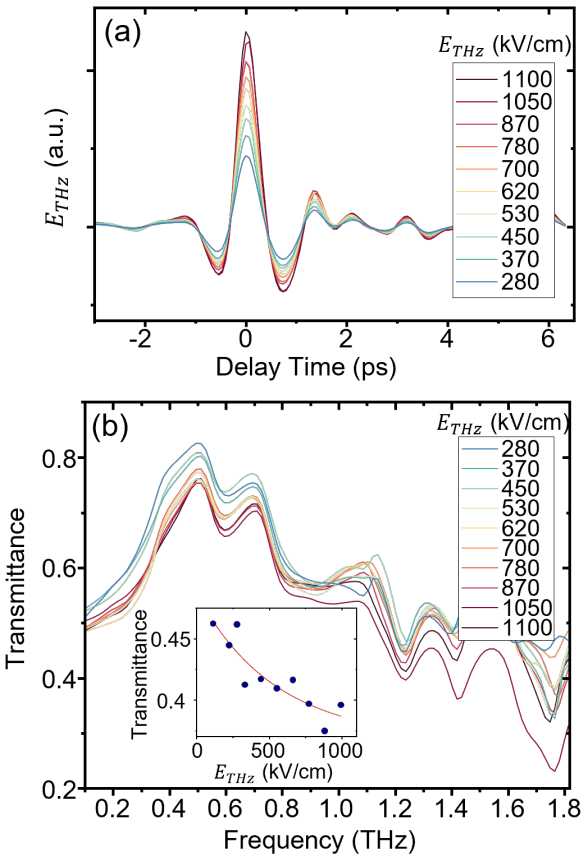

Fig. 5. (a) Waveforms transmitted through the WSe_2 sample with 400-nm, 730-$\mu J/cm^2$ optical excitation at the delay time of 3 ps and (b) the corresponding transmittance spectra. The inset shows spectrally integrated transmittance as a function of peak THz field amplitude. The sold line is a guide to the eye.

The time-resolved THz waveforms contain comprehensive information about the photocarrier dynamics in the WSe_2 sample. In particular, the transmittance spectra in Fig. 5b exhibit distinctive features such as the peaks at 0.5, 0.7, 1.1 THz and beyond, indicating that the photocarriers are not Drude-type free carriers. We extract the complex refractive index of the optically excited WSe_2, fitting the amplitude and phase spectra of the transmitted waveforms with the Fresnel

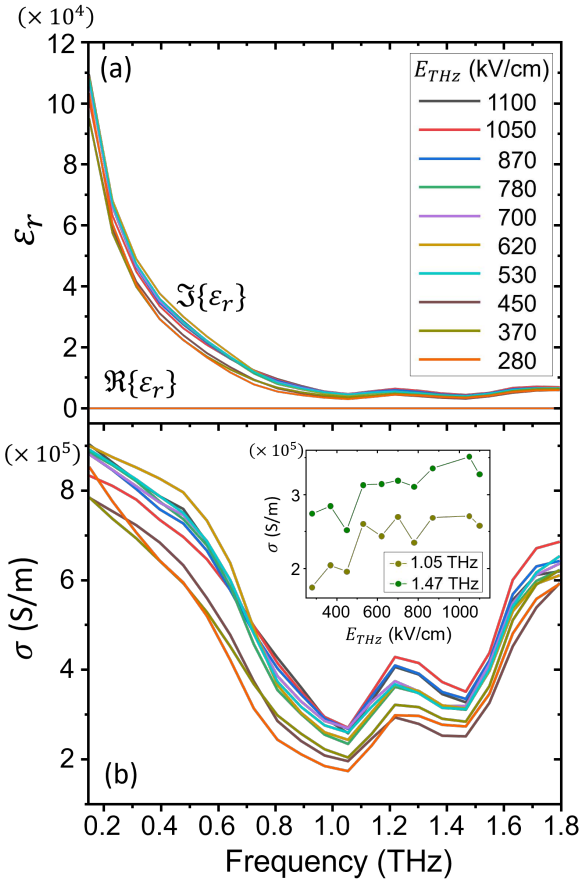

Fig. 6. (a) Spectra of the real and imaginary parts of the relative permittivity of the WSe_2 sample with 400-nm optical excitation for various THz field amplitudes. (b) Corresponding spectra of the real part of the conductivity.

transmission coefficient [48],

$$t(\omega) = \frac{t_{12}t_{23}}{t_{13}} \frac{e^{i(\tilde{n}-1)\frac{\omega L}{c}}}{1 - r_{21}r_{23}e^{2i\tilde{n}\frac{\omega L}{c}}}, \tag{1}$$

where $\tilde{n}(\omega)$ and L are the refractive index and the thickness of the multilayer WSe_2, respectively. r_{ij} and t_{ij}, where $i, j = 1, 2, 3$ for 1=air, 2=WSe_2, and 3=sapphire, are the normal-incidence Fresnel reflection and transmission coefficients. The Fresnel analysis produces the relative permittivity, $\varepsilon_r(\omega) = \tilde{n}(\omega)^2$. Figure 6a shows the spectra of the real and imaginary parts of the relative permittivity of the WSe_2 sample excited by 400-nm optical pump at various THz peak field amplitudes. The permittivity is predominantly imaginary and inversely proportional to the frequency in the low frequency region below ~0.8 THz, while the real part is flat and negligibly small compared with the imaginary part. The overall spectral features of the permittivity are consistent with the THz properties of conducting media. The optically excited WSe_2, however, is not a conventional conductor. Since the THz properties of the WSe_2 sample are dominated by the photocarriers, the relative permittivity mainly depends on the AC conductivity $\sigma(\omega)$,

$$\varepsilon_r(\omega) = \varepsilon_b(\omega) + i\frac{\sigma(\omega)}{\varepsilon_0\omega} \approx i\frac{\sigma(\omega)}{\varepsilon_0\omega}. \tag{2}$$

As shown in Fig. 6b, the complex conductivity is essentially real and increases with the THz intensity increasing. The inset shows the rising conductivity at 1.05 and 1.47 THz. The conductivity ranges from ~900,000 S/m at low frequencies, dipping down to ~200,000 S/m at 1.1 and 1.5 THz. The conductivity dips imply that the photocarriers undergo resonant interactions such as carrier-phonon scattering [49, 50].

5. Conclusion

Strong THz fields give rise to remarkable photocarrier dynamics in multilayer WSe_2. The field induced nonlinear absorption in WSe_2 is extraordinary, comparing not only with conventional 3D semiconductors such as Si, Ge and GaAs [44–47], but also with another 2D material, graphene [51, 52], in which intense THz pulses enhance transparency. Microscopic mechanisms of the nonlinear THz absorption in optically excited WSe_2 are still a work in progress. We speculate that the strong THz fields drive photocarriers into sidebands of high mobility and enhance the THz conductivity of the material. An alternative mechanism is that the strong THz fields are freeing charge carriers trapped in defect states, also resulting in the rise of the conductivity.

Funding

This work was supported by the National Science Foundation (DMR-1905634 and DMR-1720633).

Acknowledgments

The experimental work was supported by the National Science Foundation (No. DMR-1905634). Sample fabrication was supported by the NSF-MRSEC program under Award Number DMR-1720633.

Disclosures

The authors declare no conflicts of interest.

References

1. K. F. Mak, C. Lee, J. Hone, J. Shan, and T. F. Heinz, "Atomically Thin MoS_2: A New Direct-Gap Semiconductor," Phys. Rev. Lett. **105**, 136805 (2010).
2. A. Splendiani, L. Sun, Y. Zhang, T. Li, J. Kim, C.-Y. Chim, G. Galli, and F. Wang, "Emerging photoluminescence in monolayer mos2," Nano Lett. **10**, 1271–1275 (2010). PMID: 20229981.
3. D. Xiao, G.-B. Liu, W. Feng, X. Xu, and W. Yao, "Coupled Spin and Valley Physics in Monolayers of MoS_2 and Other Group-VI Dichalcogenides," Phys. Rev. Lett. **108**, 196802 (2012).
4. D. Le, A. Barinov, E. Preciado, M. Isarraraz, I. Tanabe, T. Komesu, C. Troha, L. Bartels, T. S. Rahman, and P. A. Dowben, "Spin-orbit coupling in the band structure of monolayer WSe_2," J. Phys. Condens. Matter **27**, 182201 (2015).
5. T. Cao, G. Wang, W. Han, H. Ye, C. Zhu, J. Shi, Q. Niu, P. Tan, E. Wang, B. Liu, and J. Feng, "Valley-selective circular dichroism of monolayer molybdenum disulphide," Nat. Commun. **3**, 887 (2012).
6. A. M. Jones, H. Yu, N. J. Ghimire, S. Wu, G. Aivazian, J. S. Ross, B. Zhao, J. Yan, D. G. Mandrus, D. Xiao, W. Yao, and X. Xu, "Optical generation of excitonic valley coherence in monolayer WSe_2," Nat. Nanotechnol. **8**, 634–638 (2013).
7. F. Langer, C. P. Schmid, S. Schlauderer, M. Gmitra, J. Fabian, P. Nagler, C. Schüller, T. Korn, P. G. Hawkins, J. T. Steiner, U. Huttner, S. W. Koch, M. Kira, and R. Huber, "Lightwave valleytronics in a monolayer of tungsten diselenide," Nature **557**, 76–80 (2018).
8. C.-K. Yong, M. I. B. Utama, C. S. Ong, T. Cao, E. C. Regan, J. Horng, Y. Shen, H. Cai, K. Watanabe, T. Taniguchi, S. Tongay, H. Deng, A. Zettl, S. G. Louie, and F. Wang, "Valley-dependent exciton fine structure and Autler-Townes doublets from Berry phases in monolayer $MoSe_2$," Nat. Mater. **18**, 1065–1070 (2019).
9. S. Manzeli, D. Ovchinnikov, D. Pasquier, O. V. Yazyev, and A. Kis, "2D transition metal dichalcogenides," Nat. Rev. Mater. **2**, 17033 (2017).
10. A. Ramasubramaniam, "Large excitonic effects in monolayers of molybdenum and tungsten dichalcogenides," Phys. Rev. B **86**, 115409 (2012).

11. D. Y. Qiu, F. H. da Jornada, and S. G. Louie, "Optical Spectrum of MoS_2: Many-Body Effects and Diversity of Exciton States," Phys. Rev. Lett. **111**, 216805 (2013).
12. N. Lundt, S. Klembt, E. Cherotchenko, S. Betzold, O. Iff, A. V. Nalitov, M. Klaas, C. P. Dietrich, A. V. Kavokin, S. Höfling, and C. Schneider, "Room-temperature Tamm-plasmon exciton-polaritons with a WSe_2 monolayer," Nat. Commun. **7**, 13328 (2016).
13. T. Mueller and E. Malic, "Exciton physics and device application of two-dimensional transition metal dichalcogenide semiconductors," 2D Mater. Appl. **2**, 29 (2018).
14. S. K. Pandey, R. Das, and P. Mahadevan, "Layer-dependent electronic structure changes in transition metal dichalcogenides: The microscopic origin," ACS Omega **5**, 15169–15176 (2020). PMID: 32637790.
15. Z. Sun, A. Martinez, and F. Wang, "Optical modulators with 2D layered materials," Nat. Photonics **10**, 227–238 (2016).
16. Q. H. Wang, K. Kalantar-Zadeh, A. Kis, J. N. Coleman, and M. S. Strano, "Electronics and optoelectronics of two-dimensional transition metal dichalcogenides," Nat. Nanotechnol. **7**, 699–712 (2012).
17. A. Krasnok, S. Lepeshov, and A. Alú, "Nanophotonics with 2D transition metal dichalcogenides [Invited]," Opt. Express **26**, 15972 (2018).
18. J. Shi, Z. Li, D. K. Sang, Y. Xiang, J. Li, S. Zhang, and H. Zhang, "Thz photonics in two dimensional materials and metamaterials: properties, devices and prospects," J. Mater. Chem. C **6**, 1291–1306 (2018).
19. P. Steinleitner, P. Merkl, P. Nagler, J. Mornhinweg, C. Schüller, T. Korn, A. Chernikov, and R. Huber, "Direct Observation of Ultrafast Exciton Formation in a Monolayer of WSe2," Nano Lett. **17**, 1455–1460 (2017).
20. S. Brem, M. Selig, G. Berghaeuser, and E. Malic, "Exciton Relaxation Cascade in two-dimensional Transition Metal Dichalcogenides," Sci. Reports **8**, 8238 (2018).
21. M. Selig, F. Katsch, R. Schmidt, S. Michaelis de Vasconcellos, R. Bratschitsch, E. Malic, and A. Knorr, "Ultrafast dynamics in monolayer transition metal dichalcogenides: Interplay of dark excitons, phonons, and intervalley exchange," Phys. Rev. Res. **1**, 022007 (2019).
22. C. Poellmann, P. Steinleitner, U. Leierseder, P. Nagler, G. Plechinger, M. Porer, R. Bratschitsch, C. Schüller, T. Korn, and R. Huber, "Resonant internal quantum transitions and femtosecond radiative decay of excitons in monolayer WSe_2," Nat. Mater. **14**, 889–893 (2015).
23. L. Li, M.-F. Lin, X. Zhang, A. Britz, A. Krishnamoorthy, R. Ma, R. K. Kalia, A. Nakano, P. Vashishta, P. Ajayan, M. C. Hoffmann, D. M. Fritz, U. Bergmann, and O. V. Prezhdo, "Phonon-Suppressed Auger Scattering of Charge Carriers in Defective Two-Dimensional Transition Metal Dichalcogenides," Nano Lett. **19**, 6078–6086 (2019).
24. C. J. Docherty, S. D. Stranks, S. N. Habisreutinger, H. J. Joyce, L. M. Herz, R. J. Nicholas, and M. B. Johnston, "An ultrafast carbon nanotube terahertz polarisation modulator," J. Appl. Phys. **115**, 203108 (2014).
25. J. H. Strait, P. Nene, and F. Rana, "High intrinsic mobility and ultrafast carrier dynamics in multilayer metal-dichalcogenide MoS_2," Phys. Rev. B **90**, 245402 (2014).
26. C. H. Lui, A. J. Frenzel, D. V. Pilon, Y. H. Lee, X. Ling, G. M. Akselrod, J. Kong, and N. Gedik, "Trion-Induced Negative Photoconductivity in Monolayer MoS_2," Phys. Rev. Lett. **113**, 166801 (2014).
27. S. Kar, Y. Su, R. R. Nair, and A. K. Sood, "Probing photoexcited carriers in a few-layer mos2 laminate by time-resolved optical pump-terahertz probe spectroscopy," ACS Nano **9**, 12004–12010 (2015).
28. J. K. Gustafson, P. D. Cunningham, K. M. McCreary, B. T. Jonker, and L. M. Hayden, "Ultrafast carrier dynamics of monolayer ws2 via broad-band time-resolved terahertz spectroscopy," The J. Phys. Chem. C **123**, 30676–30683 (2019).
29. S. Kar, J. Lake, S. Adeyemo, T. Santra, and H. Joyce, "The physics of terahertz negative photoconductivity in low-dimensional materials," Mater. Today Phys. **23**, 100631 (2022).
30. Y. Cao, S. Gan, Z. Geng, J. Liu, Y. Yang, Q. Bao, and H. Chen, "Optically tuned terahertz modulator based on annealed multilayer MoS_2," Sci. Reports **6**, 22899 (2016).
31. P. Gopalan, A. Chanana, S. Krishnamoorthy, A. Nahata, M. A. Scarpulla, and B. Sensale-Rodriguez, "Ultrafast THz modulators with WSe2 thin films [Invited]," Opt. Mater. Express **9**, 826 (2019).
32. Z. Fan, Z. Geng, W. Fang, X. Lv, Y. Su, S. Wang, J. Liu, and H. Chen, "Characteristics of transition metal dichalcogenides in optical pumped modulator of terahertz wave," AIP Adv. **10**, 045304 (2020).
33. F. Zhang, H. Zhang, S. Krylyuk, C. A. Milligan, Y. Zhu, D. Y. Zemlyanov, L. A. Bendersky, B. P. Burton, A. V. Davydov, and J. Appenzeller, "Electric-field induced structural transition in vertical $MoTe_2$- and $Mo_{1-x}W_xTe_2$-based resistive memories," Nat. Mater. **18**, 55–61 (2019).
34. J. Zhou, H. Xu, Y. Shi, and J. Li, "Terahertz driven reversible topological phase transition of monolayer transition metal dichalcogenides," Adv. Sci. **8**, 2003832 (2021).
35. X. Dai, W. Li, T. Wang, X. Wang, and C. Zhai, "Bandstructure modulation of two-dimensional WSe_2 by electric field," J. Appl. Phys. **117**, 084310 (2015).
36. S. Haastrup, S. Latini, K. Bolotin, and K. S. Thygesen, "Stark shift and electric-field-induced dissociation of excitons in monolayer MoS_2 and h BN /MoS_2 heterostructures," Phys. Rev. B **94**, 041401 (2016).
37. A. D. Jameson, J. L. Tomaino, Y. S. Lee, G. Khitrova, H. M. Gibbs, C. N. Böttge, A. C. Klettke, M. Kira, and S. W. Koch, "Direct measurement of light-matter energy exchange inside a microcavity," Optica **1**, 276 (2014).
38. A. Mousavian, B. Lee, A. D. Stickel, V. Brequigny, J. A. Meyers, A. N. Bradley, and Y.-S. Lee, "Terahertz-driven ultrafast recovery of plasmon resonance in photoexcited nanoantennas on GaAs," Appl. Phys. Lett. **113**, 171103 (2018).

39. J. Shi, E. Baldini, S. Latini, S. A. Sato, Y. Zhang, B. C. Pein, P.-C. Shen, J. Kong, A. Rubio, N. Gedik, and K. A. Nelson, "Room Temperature Terahertz Electroabsorption Modulation by Excitons in Monolayer Transition Metal Dichalcogenides," Nano Lett. **20**, 5214–5220 (2020).
40. B. Lee, A. Mousavian, M. J. Paul, Z. J. Thompson, A. D. Stickel, D. R. McCuen, E. Y. Jang, Y. H. Kim, J. Kyoung, D.-S. Kim, and Y.-S. Lee, "Anisotropic high-field terahertz response of free-standing carbon nanotubes," Appl. Phys. Lett. **108**, 241111 (2016).
41. J. Yang, X. Wen, H. Xia, R. Sheng, Q. Ma, J. Kim, P. Tapping, T. Harada, T. W. Kee, F. Huang, Y.-B. Cheng, M. Green, A. Ho-Baillie, S. Huang, S. Shrestha, R. Patterson, and G. Conibeer, "Acoustic-optical phonon up-conversion and hot-phonon bottleneck in lead-halide perovskites," Nat. Commun. **8**, 14120 (2017).
42. T. Wang, T. R. Hopper, N. Mondal, S. Liu, C. Yao, X. Zheng, F. Torrisi, and A. Bakulin, "Hot carrier cooling and trapping in atomically thin ws_2 probed by three-pulse femtosecond spectroscopy," ACS Nano. **17**, 6330–6340 (2023).
43. J.-H. Kim, M. R. Bergren, J. C. Park, S. Adhikari, M. Lorke, T. Frauenheim, D.-H. Choe, B. Kim, H. Choi, T. Gregorkiewicz, and Y. H. Lee, "Carrier multiplication in van der Waals layered transition metal dichalcogenides," Nat. Commun. **10**, 5488 (2019).
44. H. Y. Hwang, S. Fleischer, N. C. Brandt, J. Perkins, Bradford G., M. Liu, K. Fan, A. Sternbach, X. Zhang, R. D. Averitt, and K. A. Nelson, "A review of non-linear terahertz spectroscopy with ultrashort tabletop-laser pulses," J. Mod. Opt. **62**, 1447–1479 (2015).
45. L. Razzari, F. H. Su, G. Sharma, F. Blanchard, A. Ayesheshim, H.-C. Bandulet, R. Morandotti, J.-C. Kieffer, T. Ozaki, M. Reid, and F. A. Hegmann, "Nonlinear ultrafast modulation of the optical absorption of intense few-cycle terahertz pulses in *n*-doped semiconductors," Phys. Rev. B **79**, 193204 (2009).
46. G. Sharma, I. Al-Naib, H. Hafez, R. Morandotti, D. G. Cooke, and T. Ozaki, "Carrier density dependence of the nonlinear absorption of intense thz radiation in gaas," Opt. Express **20**, 18016–18024 (2012).
47. J. Degert, M. Tondusson, V. Freysz, E. Abraham, S. Kumar, and E. Freysz, "Ultrafast, broadband and tunable terahertz reflector and neutral density filter based on high resistivity silicon," Opt. Express **30**, 18995–19004 (2022).
48. A. M. Ulatowski, L. M. Herz, and M. B. Johnston, "Terahertz Conductivity Analysis for Highly Doped Thin-Film Semiconductors," J. Infrared, Millimeter, Terahertz Waves **41**, 1431–1449 (2020).
49. D. Yadav, M. Trushin, and F. Pauly, "Thermalization of photoexcited carriers in two-dimensional transition metal dichalcogenides and internal quantum efficiency of van der Waals heterostructures," Phys. Rev. Res. **2**, 043051 (2020).
50. J. Oh, H.-T. Chang, C. T. Chen, S. Aloni, A. Schwartzberg, and S. R. Leone, "Carrier and phonon dynamics in multilayer wse2 captured by extreme ultraviolet transient absorption spectroscopy," The J. Phys. Chem. C **127**, 5004–5012 (2023).
51. M. J. Paul, B. Lee, J. L. Wardini, Z. J. Thompson, A. D. Stickel, A. Mousavian, H. Choi, E. D. Minot, and Y.-S. Lee, "Terahertz induced transparency in single-layer graphene," Appl. Phys. Lett. **105**, 221107 (2014).
52. A. Mousavian, B. Lee, A. D. Stickel, and Y.-S. Lee, "Ultrafast photocarrier dynamics in single-layer graphene driven by strong terahertz pulses," J. Opt. Soc. Am. B Opt. Phys. **35**, 1255 (2018).